Spin Wave Excitation and Propagation Properties in a Permalloy Film

2013 Jpn. J. Appl. Phys. 52 083001

(http://iopscience.iop.org/1347-4065/52/8R/083001)

Japanese Journal of Applied Physics **52** (2013) 083001 **REGULAR PAPER**
http://dx.doi.org/**10.7567/JJAP.52.083001**

Spin Wave Excitation and Propagation Properties in a Permalloy Film

Kazuto Yamanoi[1], Satoshi Yakata[2,3], Takashi Kimura[2,3], and Takashi Manago[1]*

[1]*Department of Applied Physics, Fukuoka University, Fukuoka 814-0180, Japan*
[2]*Advanced Electronics Research Division, INAMORI Frontier Research Center, Kyushu University, Fukuoka 819-0395, Japan*
[3]*CREST, Japan Science and Technology Agency, Chiyoda, Tokyo 102-0075, Japan*
E-mail: manago@fukuoka-u.ac.jp

Received March 12, 2013; accepted June 4, 2013; published online July 18, 2013

Spin wave excitation and propagation properties in a permalloy were investigated using a vector network analyzer for the magnetostatic surface wave (MSSW) and magnetostatic backward volume wave (MSBVW) configurations. In the MSSW configuration, the excitation and transmission spectra show many peaks. They originate at the distance of antenna lines of the coplanar waveguide, and the waveguide design is important for selecting the excitation and transmission wave vectors of the spin wave. The attenuation length of the MSSW was estimated to be 7.1 μm, and the group velocity of the MSSW with a wave number of 0.26 μm^{-1} was estimated to be about 8.6 μm/ns for an external magnetic field of 20 mT. In the MSBVW configuration, however, the excitation spin wave spectrum shows a single peak, since many quantized peaks overlap. A transmission signal with a single peak was also detected, but this could be an artifact such as an induced current.

1. Introduction

Progress in spin current research[1–9] has led to various spintronic applications such as race track memory,[10,11] spin torque diodes,[12,13] spin torque oscillators,[14–16] and so on. In these studies, the carriers of the spin current are spin-polarized electrons that flow in ferromagnetic metals or are injected from ferromagnetic metals to nonmagnetic metals. Recently, spin pumping[17,18] and spin Seebeck effects[19,20] have attracted attention for the generation of a pure spin current, but these are also based on the motion of spin-polarized electrons. The diffusion length of the spin current by conduction electrons is more or less 1 μm because of the spin flip caused by the thermal effect or spin orbit interaction. A spin wave that conveys spin information can also be called a spin current without the flow of spin-polarized electrons. The advantage of the spin wave is its long-range propagation over a millimeter scale in yttrium iron garnet (YIG), and over a 10 μm scale in a permalloy (Py),[21] which is much larger than the spin diffusion length of the charge spin current. Additionally, spin wave devices are expected to be ultrafast logical gate devices.[22–24] There have been many studies using YIG for microwave devices, but metals such as Py were not satisfactory in spite of being important for integration with a Si process for spintronic devices. The first study of spin wave propagation spectroscopy for Py, which shows that magnetostatic surface waves propagate as far as 40 μm in Py, was reported by Bailleul et al.[21] Time-resolved measurement of spin wave propagation using a pulse excitation method was also reported.[25] Recently, it has been found that spin-polarized current can induce the Doppler shift of a spin wave.[26–28] The basic propagation properties in metallic films, however, are still not very clear. They will be important for future applications.[22–24] In this paper, we report spin excitation and propagation properties of a continuous sinusoidal wave using a vector network analyzer in detail.

2. Experimental Procedure

A 30-nm-thick Py thin film with a width of 100 μm was fabricated on a Si/SiO_2 substrate by sputtering, e-beam lithography, and wet etching. These were covered with a 35-nm-thick SiO_2 sputtered film for insulation, and a pair of coplanar waveguides (CPWs) for excitation and detection antennas was formed by depositing a 300-nm-thick Cu above the Py film by e-beam lithography, e-beam evaporation, and a liftoff technique. Figure 1 shows a scanning electron microscopy (SEM) image of the sample. The CPWs were of the signal-ground (SG) type and were connected at the end of electrical pads. The line width of the antenna was 2 μm, and the distance between centers of the signal and ground lines was 7 μm. The space w between the two CPWs, defined in Fig. 1, was varied from 10 to 100 μm.

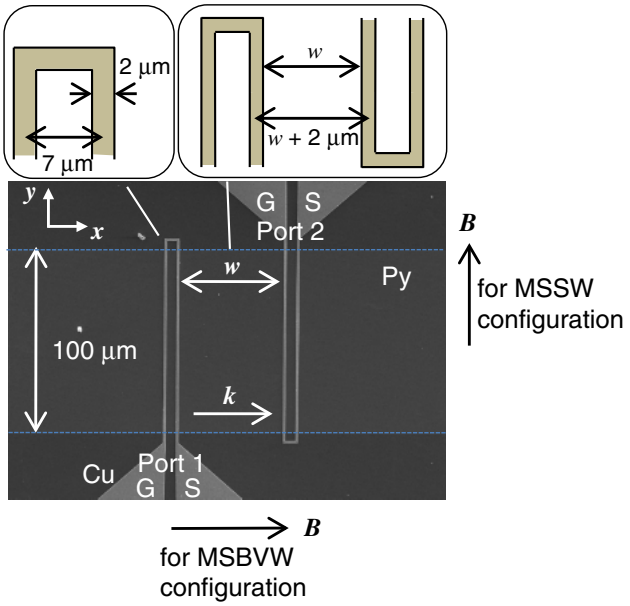

Fig. 1. (Color online) SEM image of the sample. The space between the two CPWs, w, was varied from 10 to 100 μm.

Spin wave excitation and transmission measurements were performed using a vector network analyzer (VNA; HP8510C) and a microprobe station (Cascade Microtech Summit 9000), which was modified to apply an in-plane static magnetic field. Two types of configuration were used for these measurements, depending on the relative orienta-

tions of the magnetization direction $\boldsymbol{M}$ and in-plane wave vector $\boldsymbol{k}$. As is shown in Fig. 1, one is the MSSW configuration, where the external magnetic field is applied along the y-axis and $\boldsymbol{k}$ is along the x-axis, resulting in $\boldsymbol{M} \perp \boldsymbol{k}$. The other is the MSBVW configuration, where the external magnetic field is applied along the x-axis and $\boldsymbol{k}$ is along the x-axis, resulting in $\boldsymbol{M} \parallel \boldsymbol{k}$. The dispersion relationships between frequency and wave vector for these configurations[29,30] are

$$f = \frac{\gamma}{2\pi}\sqrt{B(B+M_s) + \left(\frac{M_s}{2}\right)^2 (1 - e^{-2kd})} \quad \text{for MSSW,} \tag{1}$$

$$f = \frac{\gamma}{2\pi}\sqrt{B\left(B + M_s\frac{1-e^{-kd}}{kd}\right)} \cong \frac{\gamma}{2\pi}\sqrt{B(B+M_s)}\ (kd \ll 1), \quad \text{for MSBVW,} \tag{2}$$

where γ is the gyromagnetic ratio, B is the static magnetic field, M_s is the saturation magnetization, k is the wave number, and d is the film thickness.

The spin wave was excited at the antenna of port 1, and the propagated spin wave was detected at the antenna of port 2. For spin wave excitation measurement, one-port reflection measurement was performed and the S_{11} parameter was measured. For spin wave propagation measurement, two-port transmission measurement via a Py film was performed and the S_{21} parameter was measured. The incident microwave power was 0 dBm, which was confirmed in the linear response regime judging from the power dependence of the spectral shape. Signals obtained under a static magnetic field were analyzed by subtracting the background signal obtained without magnetic field. Hereafter, we call the subtracted signals ΔS_{11} and ΔS_{21} the reflection and transmission signals, respectively. The real part of these signals was analyzed. The choice of the real part as the characteristic parameter was mainly based on the fact that it is suitable for the determination of the resonant frequency because it exhibits a peak at the resonant frequency when the phase shift is efficiently small. On-chip full two-port calibration was carried out by using a calibration wafer, and the phase shift induced by the antennas was sufficiently small, judging from the shape of the approximately symmetric spectra of $\mathrm{Re}\,\Delta S_{11}$ in the MSBVW configuration. All measurements were performed at room temperature.

3. Results and Discussion

3.1 MSSW configuration

Figure 2(a) shows the reflection spectra ($\mathrm{Re}\,\Delta S_{11}$) under various external magnetic fields for the configuration. There are some peaks, and the interval between peaks decreases with increasing magnetic field. In our antenna configuration, the signal and ground lines are shorted, and then the spin wave excitation occurs under both the signal and ground lines almost simultaneously. Therefore, a boundary condition is given and a standing wave is excited to maximize the amplitude under both the signal and ground lines. Assuming that l is the length determined by this boundary condition, the wave number is given by $k = n\pi/l$, where n is the mode number. The peaks in the spectra correspond to the spin wave signals with different wave numbers. Such MSSW excitation with a specific wave number was also demonstrated using a resonator structure of an excitation antenna.[31,32] The peak frequency is shown as a function of magnetic field in Fig. 2(b). The solid lines are the fitting curves with the dispersion relation of MSSW [Eq. (1)]. The parameters used are $M_s = 1.08$ T and $\gamma/2\pi = 29.7$ GHz/T. The obtained wave numbers k and $l = n\pi/k$ are summarized in Table I. The value of l of 5.7–7.7 μm is appropriate for our antenna geometry, because the distance between the signal and ground lines is 7 μm, as illustrated in Fig. 2(c). The origin of the decrease in l with increasing n is not clear. It alludes to the necessity of effective boundary conditions similar to the effective "pinning" boundary conditions in confined magnetic structures.[33] Thus, an MSSW was

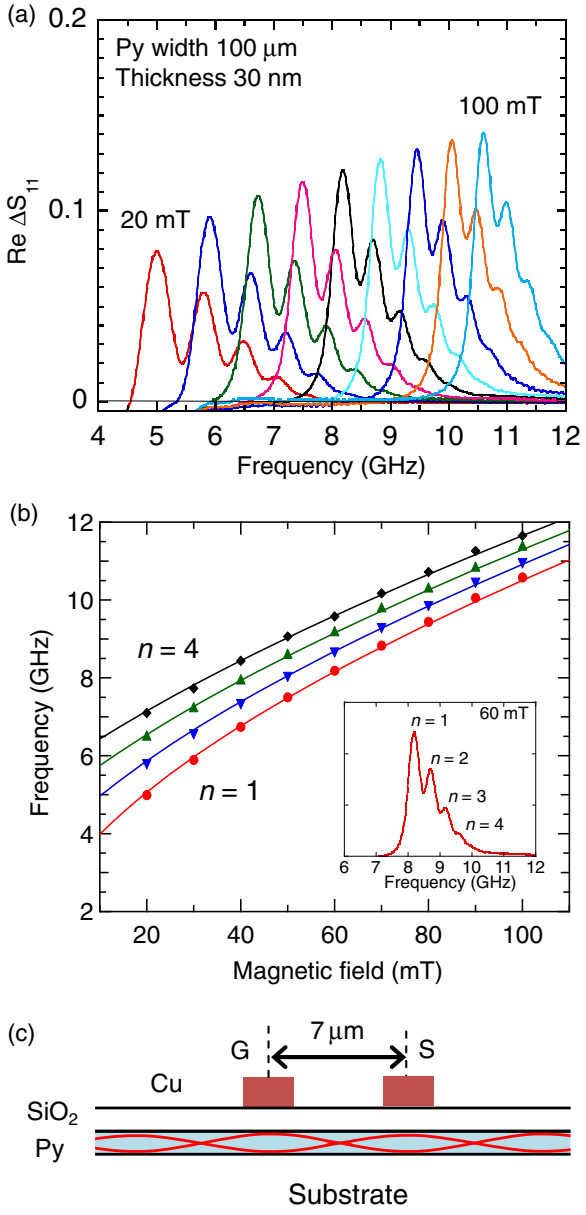

Fig. 2. (Color online) (a) Reflection spectra ($\mathrm{Re}\,\Delta S_{11}$) in MSSW configuration. (b) Dispersion relationship of the reflection signal. The solid lines are the fitting curves with the dispersion relation of the MSSW [Eq. (1)]. (c) Schematic cross section of the sample. The standing wave arises between the signal and ground lines.

Table I. Fitted results of wave numbers and related values obtained from relationship between frequency and magnetic field for MSSW.

Port 1 (S_{11} reflection measurement)

n	k (1/μm)	$l = n\pi/k$ (μm)	kd
1	0.41 ± 0.02	7.7 ± 0.4	0.012
2	1.01 ± 0.02	6.3 ± 0.2	0.030
3	1.60 ± 0.02	5.9 ± 0.1	0.048
4	2.20 ± 0.03	5.7 ± 0.1	0.066

Port 2 (S_{21} transmission measurement)

n	k (1/μm)	$l = n\pi/k$ (μm)	kd
1	0.26 ± 0.02	11.9 ± 0.9	0.008
2	0.55 ± 0.03	11.5 ± 0.6	0.016
3	0.93 ± 0.03	10.2 ± 0.3	0.028
4	1.20 ± 0.03	10.4 ± 0.3	0.036
5	1.59 ± 0.03	9.9 ± 0.2	0.048

successfully excited in this configuration. Note that spin waves with not only the wave number corresponding to the peak frequency but also various wave numbers are excited, since the spectra are spread over a wide frequency range.

The transmission spectra ($\mathrm{Re}\,\Delta S_{21}$) for $w = 10\,\mu\mathrm{m}$ are shown in Fig. 3(a). The peak frequency of $\mathrm{Re}\,\Delta S_{21}$ is not the same as that of $\mathrm{Re}\,\Delta S_{11}$, and its oscillation is fine. Figure 3(b) shows the magnetic field dependence of peak frequency. Peak indexes were determined and are shown in the inset of Fig. 3(b). Some peaks have a shoulder or become slightly broad. It seems that the peak shape is affected by that of the excitation spectra, because $\mathrm{Re}\,\Delta S_{11}$ has a local minimum around the frequency where $\mathrm{Re}\,\Delta S_{21}$ becomes broad or has a shoulder. Therefore, we eliminate the shoulderlike peak to fix the indexes. The fitting curves of $n = 1$–5 of the MSSW [Eq. (1)] are also shown, and the fitted results are indicated in Table I. The obtained l is approximately 12 μm, which is roughly in agreement with the distance between the excitation and detection antennas, as illustrated in Fig. 3(c), although a decrease in l with n is observed similarly to the result of S_{11} analysis. As shown in a snapshot image of the spin wave [Fig. 3(c)], a large spin wave signal can be detected when the magnetization modulation is large under the detection antenna. This is explained as follows. The S parameter is defined by $S_{21} = S_2/S_1 = |S_2|\exp i\theta_2/|S_1|\exp i\theta_1 = |S_2|/|S_1|\exp i(\theta_2 - \theta_1)$, where S_1 is the incident signal and S_2 is the detected signal. When $\theta_2 - \theta_1 = 2n\pi$, $\mathrm{Re}\,S_{21}$ becomes maximum. This means that the propagation wave should have the maximum amplitude under the detection antenna when the incident wave has the maximum amplitude under the incident antenna in the snapshot image. Therefore, when the wavelength matches the distance between the excitation and detection antennas, the detection antenna can pick up the real part of the spin wave signal effectively. Thus, we can analyze the multipeak spectra similarly to in standing wave analysis. The transmission properties of the spin wave depend on the distance between the two antennas, though a standing wave does not arise between the two antennas of

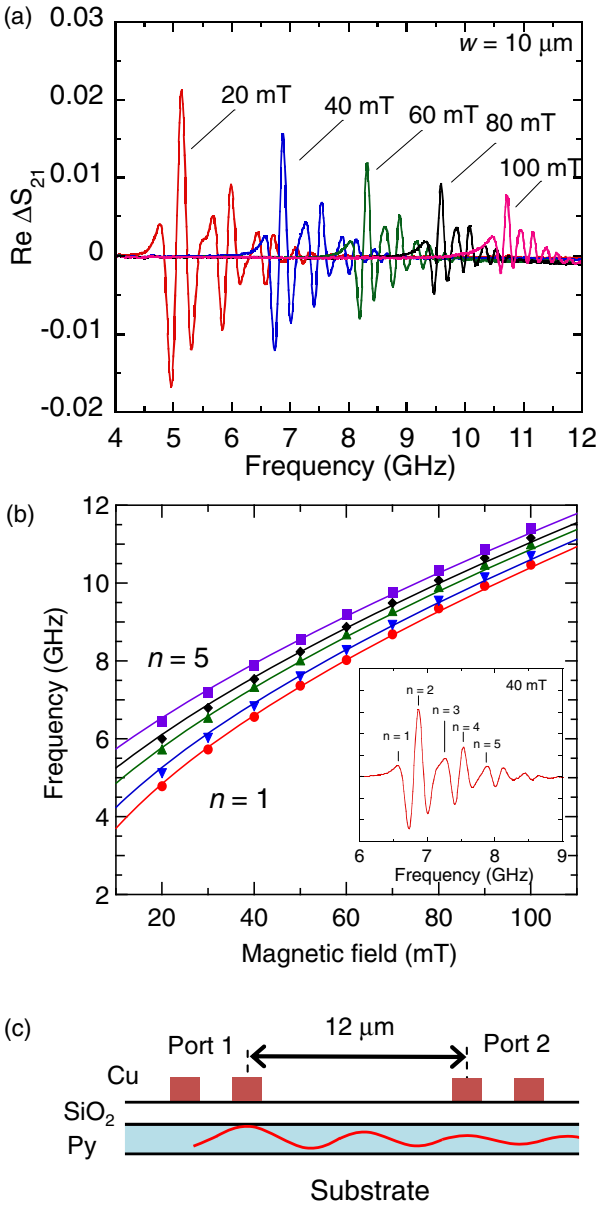

Fig. 3. (Color online) (a) Transmission spectra ($\mathrm{Re}\,\Delta S_{21}$) for $w = 10\,\mu\mathrm{m}$ in MSSW configuration. (b) Dispersion relationship of the transmission signal. The fitting curves with the dispersion relation of the MSSW [Eq. (1)] are also shown. The inset shows the peak indexes of the signal. (c) Schematic cross section of the sample and the efficiently detectable spin waves.

ports 1 and 2. This result shows the possibility of realizing a wave vector filter by controlling the distance between the antennas.

Figure 4(a) shows the transmission spectra ($\mathrm{Re}\,\Delta S_{21}$) for various w under an external field of 20 mT. The spin wave signal can be seen up to 40–50 μm, which is consistent with the previous reports.[21,28] The signal intensity is defined as the largest peak-to-peak value, and plotted as a function of w in Fig. 4(b). The inset of Fig. 4(b) shows the same data with a semi-logarithmic scale. The intensity decreases exponentially and the attenuation length of the MSSW was estimated to be 7.1 μm.

Since the spin wave with a different k is clearly observed owing to the oscillation of the spectrum, one can the deduced group velocity of the spin wave from the interval

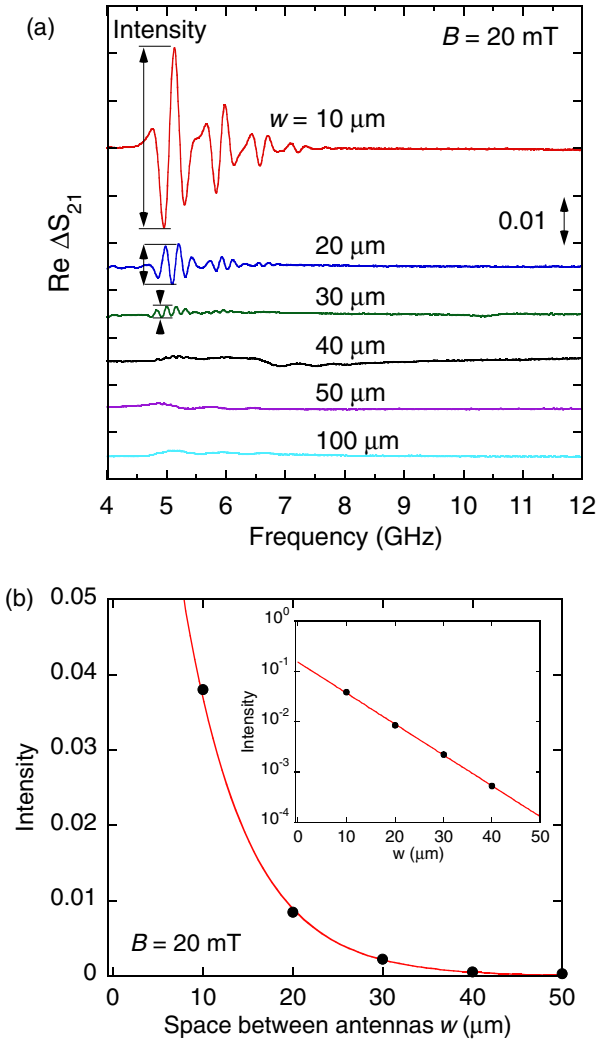

Fig. 4. (Color online) (a) Transmission spectra (Re ΔS_{21}) for various w under external field of 20 mT. (b) Signal intensity as a function of w. The inset shows the same data with a semi-logarithmic scale. The attenuation length of the MSSW was estimated to be 7.1 μm.

between the peaks of the spectrum. The group velocity of the MSSW with wave number k is theoretically expressed as

$$v_g = \frac{d\omega}{dk} = \gamma\left(\frac{M_s}{2}\right)^2 \frac{d\exp(-2kd)}{\sqrt{B(B+M_s)+\left(\frac{M_s}{2}\right)^2(1-e^{-2kd})}}. \quad (3)$$

The v_g depends on $k = n\pi/l$, that is, the index of n. When $n = 1$, v_g is calculated to be 9.9 μm/ns for $w = 10$ μm ($l = 12$ μm) and $B = 20$ mT. Experimentally, one can use two neighboring peaks of the spectrum ($\Delta n = 1$),

$$v_g = \frac{\Delta\omega}{\Delta k} = \frac{2\Delta f}{\Delta n/l} = 2l\Delta f. \quad (4)$$

In the case of $w = 10$ μm ($l = 11.9$ μm: experimental value) and $B = 20$ mT, the group velocity of $n = 1$ is deduced to be approximately 8.6 μm/ns using the frequency difference Δf between the first peak ($n = 1$) and the second peak ($n = 2$), which is in close agreement with the theoretical group velocity of 9.9 μm/ns.

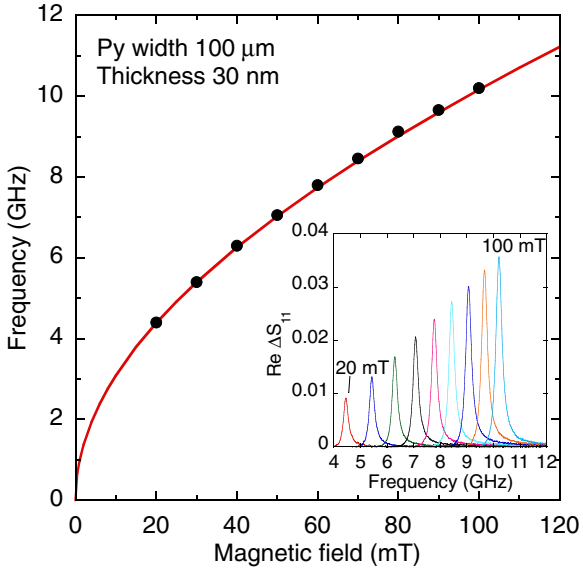

Fig. 5. (Color online) Dispersion relationship of reflection signal in MSBVW configuration. The inset shows the reflection spectra (Re ΔS_{11}) of the MSBVW configuration.

3.2 MSBVW configuration

Figure 5 shows the relationship between the peak frequency of the reflection spectra and the external magnetic field, and the inset shows the reflection spectra (Re ΔS_{11}) under various magnetic fields for the MSBVW configuration. Only a single peak was obtained for each magnetic field. Since kd is much smaller than unity, as shown in Table I, the dispersion relation of the MSBVW [Eq. (2)] becomes the same as Kittel's equation for thin films. Therefore, even if many standing waves are excited, their quantized peaks overlap, and consequently only one peak is observed. The solid curve shows the result calculated using Eq. (2), which is in good agreement with the experimental result.

Regarding the transmitted property shown in Fig. 6(a), a similar dispersion relation is obtained, compared with the reflection properties of the MSBVW. The intensity of the spectra, however, is much lower than that of the MSSW signals. As shown in Fig. 3(a) for the MSSW, the signal intensity decreases with increasing magnetic field because the damping term in the LLG equation increases with increasing magnetic field. On the other hand, for the transmission signal in the MSBVW configuration, the intensity increases with increasing magnetic field, as shown in the inset of Fig. 6(a). It seems that the intensity increase observed in the reflection spectra in the inset of Fig. 5 affects the transmission signal. It is, however, not clear why the intensity of the reflection spectra increases with the magnetic field at present. Additionally, Fig. 6(b) shows that the intensity of the transmission signal does not depend on the distance between the antennas. If this is the MSBVW signal, it should decrease with increasing distance between the antennas because of the decay. Therefore, we considered that these spectra are *not* attribute to the MSBVW propagation, and could reflect a kind of induced current in a Py strip. Further investigation is necessary for an MSBVW in metallic films.

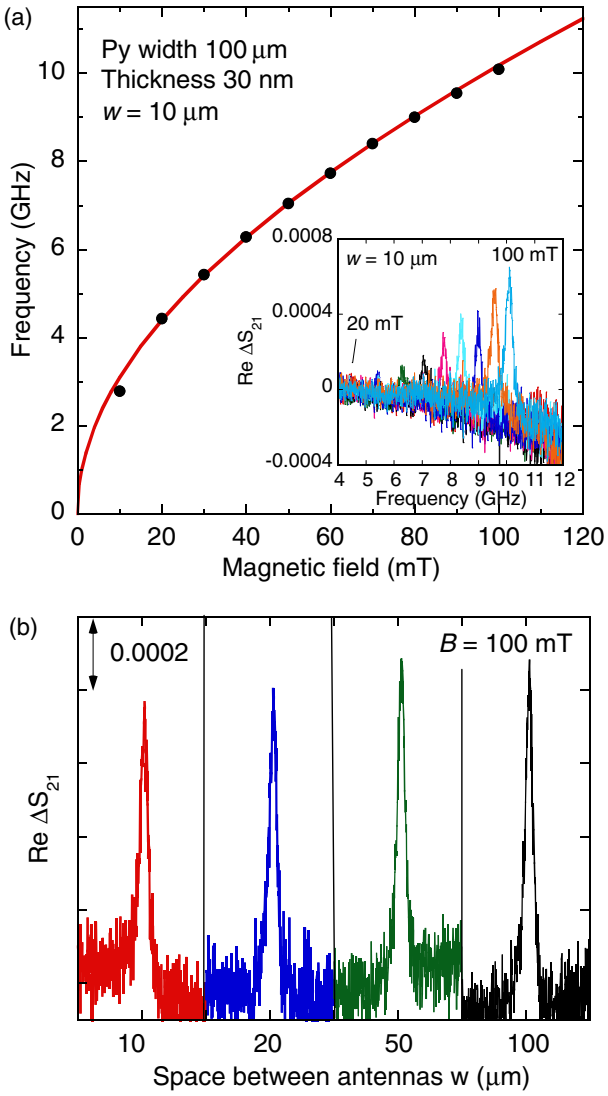

Fig. 6. (Color online) (a) Dispersion relationship of transmission signal in MSBVW configuration. The inset shows the transmission spectra (Re ΔS_{21}) of the MSBVW configuration. (b) Antenna distance dependence of Re ΔS_{21}.

4. Conclusion

We investigated the spin wave excitation and propagation properties of a continuous sinusoidal wave using a VNA. In the MSSW configuration, the excited spin wave spectra show some peaks, owing to the standing wave excitation between signal and ground lines. The transmission spin wave spectra also show many peaks in contrast to the excited spin wave spectra. The peaks depend on the distance between the antennas of the two ports. These properties suggest that the distance between the antennas can control the wave vector of the transmitted spin wave; thus, they can be used as a wave vector filter. The attenuation length of the MSSW was estimated to be 7.1 μm, and the group velocity of $n = 1$ was deduced to be approximately 8.6 μm/ns for $B = 20$ mT. In the MSBVW configuration, the excited spin wave spectra show a single peak for each magnetic field. This is due to the overlapping of many quantized peaks because of a very small kd. The transmission signal does not depend on the antenna distance. Therefore, this result implies that the transmission signal does not originate from the MSBVW, and it could indicate a kind of induced current. One should thus take care in the MSBVW measurement using a VNA.

Acknowledgments

This work was partly supported by JSPS KAKENHI Grant Number 24560034. This work was partly supported by funds (Nos. 115002 and 127005) from the Central Research Institute of Fukuoka University. The authors thank Dr. Kasai of the National Institute for Materials Science (NIMS) for fruitful discussions.

1) J. C. Slonczewski: J. Magn. Magn. Mater. **159** (1996) L1.
2) L. Berger: Phys. Rev. B **54** (1996) 9353.
3) J. A. Katine, F. J. Albert, R. A. Buhrman, E. B. Myers, and D. C. Ralph: Phys. Rev. Lett. **84** (2000) 3149.
4) F. J. Jedema, A. T. Filip, and B. J. van Wees: Nature **410** (2001) 345.
5) A. Yamaguchi, T. Ono, S. Nasu, K. Miyake, K. Mibu, and T. Shinjo: Phys. Rev. Lett. **92** (2004) 077205.
6) M. Zaffalon and B. J. van Wees: Phys. Rev. B **71** (2005) 125401.
7) T. Kimura, Y. Otani, and J. Hamrle: Phys. Rev. Lett. **96** (2006) 037201.
8) S. O. Valenzuela and M. Tinkham: J. Appl. Phys. **101** (2007) 09B103.
9) T. Yang, T. Kimura, and Y. Otani: Nat. Phys. **4** (2008) 851.
10) S. S. P. Parkin, M. Hayashi, and L. Thomas: Science **320** (2008) 190.
11) M. Hayashi, L. Thomas, R. Moriya, C. Rettner, and S. S. P. Parkin: Science **320** (2008) 209.
12) A. A. Tulapurkar, Y. Suzuki, A. Fukushima, H. Kubota, H. Maehara, K. Tsunekawa, D. D. Djayaprawira, N. Watanabe, and S. Yuasa: Nature **438** (2005) 339.
13) Y. Suzuki and H. Kubota: J. Phys. Soc. Jpn. **77** (2008) 031002.
14) R. Matsumoto, A. Chanthbouala, J. Grollier, V. Cros, A. Fert, K. Nishimura, Y. Nagamine, H. Maehara, K. Tsunekawa, A. Fukushima, and S. Yuasa: Appl. Phys. Express **4** (2011) 063001.
15) S. Kaka, M. R. Pufall, W. H. Rippard, T. J. Silva, S. E. Russek, and J. A. Katine: Nature **437** (2005) 389.
16) A. D. Belanovsky, N. Locatelli, P. N. Skirdkov, F. A. Araujo, J. Grollier, K. A. Zvezdin, V. Cros, and A. K. Zvezdin: Phys. Rev. B **85** (2012) 100409(R).
17) A. Brataas, Y. Tserkovnyak, G. E. W. Bauer, and B. I. Halperin: Phys. Rev. B **66** (2002) 060404(R).
18) E. Saitoh, M. Ueda, H. Miyajima, and G. Tatara: Appl. Phys. Lett. **88** (2006) 182509.
19) K. Uchida, S. Takahashi, K. Harii, J. Ieda, W. Koshibae, K. Ando, S. Maekawa, and E. Saitoh: Nature **455** (2008) 778.
20) J. Xiao, G. E. W. Bauer, K. Uchida, E. Saitoh, and S. Maekawa: Phys. Rev. B **81** (2010) 214418.
21) M. Bailleul, D. Olligs, C. Fermon, and S. O. Demokritov: Europhys. Lett. **56** (2001) 741.
22) M. P. Kostylev, A. A. Serga, T. Schneider, B. Leven, and B. Hillebrands: Appl. Phys. Lett. **87** (2005) 153501.
23) K.-S. Lee and S.-K. Kim: J. Appl. Phys. **104** (2008) 053909.
24) T. Schneider, A. A. Serga, B. Leven, B. Hillebrands, R. L. Stamps, and M. P. Kostylev: Appl. Phys. Lett. **92** (2008) 022505.
25) M. Covington, T. M. Crawford, and G. J. Parker: Phys. Rev. Lett. **89** (2002) 237202.
26) V. Vlaminck and M. Bailleul: Science **322** (2008) 410.
27) M. Zhu, C. L. Dennis, and R. D. McMichael: Phys. Rev. B **81** (2010) 140407(R).
28) K. Sekiguchi, K. Yamada, S.-M. Seo, K.-J. Lee, D. Chiba, K. Kobayashi, and T. Ono: Phys. Rev. Lett. **108** (2012) 017203.
29) A. N. Slavin, S. O. Demokritov, and B. Hillebrands: in *Spin Dynamics in Confined Magnetic Structures I*, ed. B. Hillebrands and K. Ounadjela (Springer, Berlin, 2002) p. 36.
30) S. O. Demokritov and B. Hillebrands: in *Spin Dynamics in Confined Magnetic Structures I*, ed. B. Hillebrands and K. Ounadjela (Springer, Berlin, 2002) p. 65.
31) V. Vlaminck and M. Bailleul: Phys. Rev. B **81** (2010) 014425.
32) K. Kiseki, S. Yakata, and T. Kimura: Appl. Phys. Lett. **101** (2012) 212404.
33) K. Y. Guslienko, S. O. Demokritov, B. Hillebrands, and A. N. Slavin: Phys. Rev. B **66** (2002) 132402.